Overview of the First SMOS Sea Surface Salinity Products. Part I: Quality Assessment for the Second Half of 2010

Nicolas Reul[1,*], Joseph Tenerelli[2], Jaqueline Boutin[3], Bertrand Chapron[1], Frédéric Paul[1], Emilie Brion[4], Fabienne Gaillard[1], and Olivier Archer[1]

[1] Institut Français de Recherche pour l'Exploitation de la Mer (IFREMER), Laboratoire d'Océanographie spatiale, 29280 Plouzané, France, F. Gaillard : Laboratoire de Physique des Océans
[2] Collect Localisation Satellite, Radar division, Plouzané, France
[3] Institut Pierre-Simon Laplace, Laboratoire d'Océanographie et du Climat—Expérimentation et Approches Numériques (LOCEAN), Unité Mixte de Recherche Université Pierre et Marie Curie–Centre National de la Recherche Scientifique–Institut de Recherche pour le Développement–Muséum National d'Histoire Naturelle, Paris, 75252 France
[4] Atlantide-Altran Ouest, Technopôle Brest Iroise Site du Vernis – CS 23866 29238 Brest Cedex 3

*: Corresponding author : N. Reul, email address : Nicolas.Reul@ifremer.fr

Abstract:

Multi-angular images of the brightness temperature $(T_{\rm B})$ of the Earth at 1.4 GHz are reconstructed from the Soil Moisture and Ocean Salinity (SMOS) satellite sensor data since end 2009. Sea surface salinity (SSS) products remote sensing from space is being attempted using these data over the world oceans. The quality of the first version of the European Space Agency operational Level 2 (L2) SSS swath products is assessed in this paper, using satellite/in situ SSS data match-ups that were collected over the second half of 2010. This database reveals that 95% of the SMOS L2 products show a global error standard deviation on the order of $\sim$1.3 practical salinity scale. Simple spatiotemporal aggregation of the L2 products to generate monthly SSS maps at $1^{\circ} \times 1^{\circ}$ spatial resolution reduces the error down to about 0.6 globally and 0.4 in the tropics for 90% of the data. Several major problems are, however, detected in the products. Systematically, SMOS SSS data are biased within a $\sim$1500 km wide belt along the world coasts and sea ice edges, with a contamination intensity and spread varying from ascending to descending passes. Numerous world ocean areas are permanently or intermittently contaminated by radio-frequency interferences, particularly in the northern high latitudes and following Asia coastlines. Moreover, temporal drifts in the retrieved SSS fields are found with varying signatures in ascending and descending passes. In descending passes, a time-dependent strong latitudinal bias is found, with maximum amplitude reached at the end of the year. Errors in the forward modeling of the wind-induced emissivity and of the sea surface scattered galactic sources are as well identified, biasing the sss retrievals at high and low winds and when the galactic equator sources are reflected toward the sensor.

Keywords: L-Band, Microwave Radiometry, Ocean Salinity, Sea Surface.

I.   <u>Introduction</u>

One of the key goals of the European Space Agency's (ESA) Soil Moisture and Ocean Salinity (SMOS) mission, launched in November 2009, is to produce global maps of Sea Surface Salinity (SSS) with an accuracy of 0.1-0.2 (on the Practical Salinity Scale 1978) over a time scale of 1 month and at a spatial resolution of about 100 km, using measurements of upwelling L-band radiation obtained from the interferometric radiometer MIRAS (Microwave Imaging Radiometer using Aperture Synthesis). This is a challenging objective for several major reasons. First, the sensitivity of L-band brightness temperatures to variations in SSS is at best about 1 K per salinity unit (for sea surface emitted total power) obtained in the warm tropical oceans with sea surface temperature (SST) around 30°C and in Vertical-polarization at 50° incidence angle. For all incidences and polarization, the sensitivity to SSS is reduced as SST decreases. This sensitivity is very weak given that spatial and temporal variability in open-ocean SSS does not exceed several units and that the instrument noise is typically 2-5 Kelvin [1]. Second, there are many geophysical sources of brightness at L-band that corrupt the salinity signal (see [2,3] for a summary of these sources), and the scene brightness models used to account for these sources have uncertain accuracy, especially those for rough surface and foam-induced excess emissions [2,4,5], sun glint [6] and sea surface scattered galactic sources [7,8].
Moreover, the technical approach developed to achieve

adequate radiometric accuracy for the SMOS satellite, as well as spatial and temporal resolution compromising between land and ocean science requirements, is polarimetric interferometric radiometry [9,1]. It is important to recall here that this ambitious technique is used for the first time in the context of earth observation from space. The SMOS synthetic antenna MIRAS consists of 69 radiometer elements operating at L-band (frequency ~1.4 GHz) and distributed along three equally spaced arms, resulting in a planar Y-shaped structure. As compared to real aperture radiometers, in which brightness temperature (T_B) maps are obtained by a mechanical scan of a large antenna, in aperture synthesis radiometers, a T_B image is formed through Fourier synthesis from the cross correlations between simultaneous signals obtained from pairs of antenna elements, namely, the visibilities. SMOS data image processing (so-called Level 1, see [10,1] for details) thus consists in reconstructing the brightness temperatures from the non local (in the physical space) visibility measurements of the earth emitted radiations. By construction, this method introduces additional difficulties for the sea surface salinity retrievals, especially in areas showing strong brightness temperature contrasts such as land-ice/ocean/sky transitions, or in the presence of strong local sources, such as those generated by man-made radio frequency interferences, or, by the direct sun radiations impinging the antenna. As the latter signals exhibit very local sharp transitions in the physical space, they indeed generate multiple spatial frequency signatures in the Fourier domain that are superimposed with the background ocean signal. It is therefore difficult to estimate and correctly account for their impacts on the visibilities prior to reconstruction.

Finally, reaching a sufficiently accurate calibration and temporal stability to reach the objectives of the low sensitivity ocean surface salinity measurements is also a very challenging task for an instrument including 69 radiometer elements, with potentially varying individual behavior.

Prior to launch, an algorithm detailed in [11] had been developed to retrieve surface salinity from the reconstructed brightness temperatures of SMOS and is implemented in the ESA Level 2 ocean salinity operational processing chain. Briefly, the sea surface salinity retrieval algorithm is based on an iterative inversion method that minimizes the differences between antenna plane Tb measured at different incidence angles and Tb simulated by a forward radiative transfer model. The iterative method is initialized with a first-guess surface salinity that is iteratively modified until an optimal fit between the forward model and the measurements is obtained. The forward model takes into account atmospheric emission and absorption, ionospheric effects (Faraday rotation), scattering of celestial radiation by the rough ocean surface, and rough sea surface emission as approximated by one of three models. Potential degradation of the retrieval results is indicated through a flagging strategy. In particular, the flags are raised if the retrieved SSS exceed the mean climatological value plus or minus five times the climatology standard deviation.

In the first part of this paper, the quality of the current ESA operational Level 2 SSS products generated using one of the forward wind-induced excess emissivity model is analyzed. The algorithm is basically the one described in [11], except for a two-dimensional offset function, called the Ocean Target Transformation (OTT), which is now applied to the Level 1 reconstructed brightness temperatures used as inputs to the Level 2 processor, prior to the minimization with the forward model estimates. This offset function is applied to correct for systematic image reconstruction biases that were found in the data during the satellite commissioning period and serves as a calibration factor. The OTT is determined by the two-dimensional median differences between the forward model predictions estimated using the world ocean atlas monthly climatology [12] and the Level 1 (L1) reconstructed brightness temperatures. This analysis is performed in the director cosine coordinates of the antenna and involve few orbits in the Pacific ocean. Additional details with respect this calibration method can be found in [13, 14].

During the first year of the mission, and particularly during the first half of 2010, the algorithms used in the operational Level 0 (L0)-Level 1 processors and the associated calibration parameters and techniques (Flat Target Response, Noise Injection Radiometer data, thermal model, external sources removal techniques, ..) evolved significantly as the data were first recovered and further analyzed. Nevertheless, it was rapidly observed that after some empirical corrections, it was possible to derive the spatial variability of SSS from SMOS data [13]. SMOS Level 2 operational SSS products were thus obtained from a first "quasi stable" version of the L0 and L1 algorithms starting approximately in mid-2010. This led [15] to focus on SMOS SSS validation in August 2010; they found a precision on SMOS SSS averaged in 100kmx100km boxes and 10 days around 0.4 provided that SMOS SSS are weighted by their error variance and that only data in the 3-12m/s wind speed range, in open ocean regions (far from land), and on ascending orbits (to avoid potential problems associated with large galactic signal) are considered; systematic salinity differences of several tenths of units were found between ascending and descending orbits depending on the hemisphere.

In this paper, L2 SSS data quality assessment is extended over the second half of the year 2010. Two updates of the OTT were nevertheless implemented in the operational Level 2 chain at the beginning of that period to compensate for deep sky calibration changes in the Level 1. The latter changes occurred the 9th of July and the 2nd of August.

For the purpose of validating the satellite products, *in situ* SSS data were collected, validated and co-localized with SMOS data. This match-up database is used here to qualify the SMOS Level 2 swath product errors but also the ones characterizing the data after spatio-temporal aggregation of the Level 2 (so-called Level 3 SSS product). The major spatio-temporal evolution during that period and the geophysical

dependencies of the error are analyzed. Simple spatio-temporal aggregation of the Level 2 products are then performed to generate monthly Level 3 SSS maps at 1°x1° spatial resolution from July to December. The error reduction in the SMOS SSS products is analyzed and several permanent major problems detected in the products are identified and discussed. The latter include systematic SSS biases within a ~1500 km wide belt along the world coasts and sea ice edges, affecting data in both ascending and descending passes. Moreover, temporal drifts are found in the retrieved SSS, with a significant latitudinal variation observed in descending passes and reaching maximum magnitude around the winter solstice. In addition, biases induced by inaccuracies in the forward modeling of the sea surface roughness impact and of the scattered galactic noise are detected.

In part II of the paper, the potential sources for these errors observed in the retrieved SSS will be analyzed in terms of brightness temperature signatures. First, the biases along the coastlines will be shown to be induced by a contamination from land or ice masses emission impinging the extended field of view domain of the MIRAS antenna. Spatio-temporal drifts in the brightness temperature are characterized and found to be dominantly correlated with the varying impact and associated corrections of the direct sun radiation impinging at the antenna and to a lesser extent to galactic signal impact and instrument thermal response. Finally, roughness-induced excess brightness temperature are estimated at the surface Level, classified and bin-averaged as function of surface wind speed values to evaluate a new empirical roughness-correction algorithm. A detailed analysis of the biased model for the galactic reflection at the sea surface will be also provided.

II.   STUDY DATA SET

This section describes the data sets which we will be using for the analysis performed in this paper.

A.   SMOS data

SMOS T_B images are formed through Fourier synthesis from the cross correlations between simultaneous signals obtained from pairs of antenna elements. SMOS Level-1B product is the output of the image reconstruction of the observations and comprises the Fourier component of the brightness temperature in the antenna polarization reference frame, hence brightness temperatures. Level-1B corresponds to one temporal measurement, i.e. the whole field of view– one integration time – and is often called a snapshot as for a camera. As the satellite moves, multiple observations of the same pixel at different incidence angles are obtained (see Fig. 6 in [1]). The Level-1C product corresponds to a Level-1B product re-organized with the angular brightness temperatures at the top of the atmosphere grouped together. The product is geolocated in an equal-area grid system (ISEA 4H9 - Icosahedral Snyder Equal Area projection) provided at 15 km resolution. For this study, the SMOS Level 1B Ocean Full Polarization products generated by the SMOS Data Processing Ground Segment (DPGS) were used. Depending on the analysis performed, we considered T_B data reconstructed either in the Extended Field of View (EFOV) domain of the antenna or only in the restricted Alias Free Field of View (AF-FOV) for which the swath width is approximately 1200 km and 800 km, respectively. The actual spatial resolution of the reconstructed T_{BS} varies within the FOV from ~32 km at boresight to about ~80 km at the edges of the swath (43 km on average over the field of view). The probing earth incidence angle is ranging from nadir to about 60° and the radiometric resolution from 2.6 K at boresight to about 4-5 K on the swath edges. For the Level 2 SSS data, the products distributed by the DPGS were used. In addition, to evaluate the impact of several corrections applied to the visibilities (sun, foreign sources,..) in the operational Level 1 processor, a simplified image reconstruction algorithm was implemented, hereafter referred to as JRECON and will be presented in more details in part II. Note that hereafter, a pass is defined as a half-orbit, pole to pole, either ascending (northward) or descending (southward).

B.   In Situ match-up data sets

In the frame of the French project GLOSCAL (Global Ocean Surface Salinity Calibration and Validation), a contribution to SMOS calibration/validation activities, in situ SSS measurements are systematically collected and validated at IFREMER to provide quality-controlled SSS data bases over the world oceans. Based on the Coriolis datasets and using ISAS (In Situ Analysis System) objective analysis tool (see [16]), a near real time analysis system has been developed. It provides gridded fields of sea surface salinity and temperature and the corresponding in-situ dataset. Argo international array of profiling floats is the principal source of data, reporting temperature and salinity from 2000m to near surface Level (4-5m). More isolated measurements from CTDs, sensor equipped marine mammals and moorings (such as TAO/PIRATA in the tropics) complement the dataset [17]. Within the GLOSCAL context, data from surface dedicated instruments that are not yet in the Coriolis operational flow were incorporated. First priority has been put on those collected with Thermosalinographs. Quality control of these data is a prerequisite before they could be integrated to the objective analysis ISAS. The in-situ observations used to build our dataset are mainly collected and processed by the Coriolis data centre, which apply a real time quality controls in two steps. First, a set of automatic tests (location and date, spikes...) is applied to the database, followed by a visual checking. The result is that quality flags ranging from 0 (no control) to 9 (missing value) are assigned to each individual measurement. Then, after running daily objective analysis, a diagnostic test detects outliers by screening the analysis residuals.

Anomalous profiles are visually checked by an operator. For the needs of GLOSCAL, Coriolis data centre has implemented a near-real time data flow. At the beginning of each month, a new analysis is performed with the data of the previous month, thus providing a dataset of improved quality. The TSG data are collected within the context of GOSUD international project (Global Ocean Surface Underway Data). The GOSUD dataset is hosted by Coriolis that performs the project agreed real time quality controls on this dataset. For our analysis, only data that have passed delayed mode processing are used. The delayed mode quality control on TSG data is performed by the scientists from various French laboratories (LPO, LOCEAN, IRD Centers and LEGOS) using a dedicated software. There are two Levels of control: quality flags and corrections. The quality flags used follows the Coriolis definition and depends on the quality of the data with respect to the climatology, spikes, noise, etc. Then when needed, the time series are adjusted to fit the external data which can be either the water sample analysis (taken aboard) and/or the Argo co-localized data with ship tracks. The TSG data set so produced are a contribution to the GOSUD project and are available in NetCDF Gosud format.

From July to December 2010, the ensemble of *in situ* qualified SSS measurements (Argo+TSG+ moorings+CTD) found in the upper 10 meter of the world oceans include a steady averaged number of ~ 300 observations per day when spatially-averaging the data over 0.25°x0.25° boxes. The spatial distribution of this *in situ* validation dataset collected over the second half of 2010 is shown in Figure 1 a. As illustrated, the current in situ observing systems provide an excellent spatial coverage of almost all open ocean areas to validate the spaceborne measurements of SSS.

The quality-controlled *in situ* SSS data were co-localized with SMOS swath Level 2 data products using a proximity criteria defined as: distances between satellite and in situ data less than ±25 km to account for the average pixel size and time lags between both data sets less than ±12 hours. For each satellite pass-type (ascending and descending), approximately 18000 match-up data with SMOS Level 2 SSS products were found over the period July to December 2010. For the validation of the SMOS spatio-temporally aggregated data (Level 3), the ensemble of in situ data were simply averaged over the same spatio-temporal boxes than the SMOS ones.

III. ASSESMENT OF SMOS SSS DATA QUALITY

In this section, the L2 SMOS swath SSS retrieval products overall quality is first estimated over the selected period; the spatio-temporal drifts in the SMOS SSS retrievals are then analyzed and we further determine some basic geophysical dependencies in the retrieved products. Finally, an assessment of the Level 3 SSS products quality is given.

A. *Overall SMOS Level 2 SSS quality*

An example of a daily map of SMOS retrieved SSS in ascending passes is shown in Figure 1.b to illustrate the spatial coverage provided by the large SMOS swath. As well, numerous missing data can be observed locally in SMOS Level 2 SSS passes. These missing data are dominantly due to contaminated brightness temperature measurements by radio frequency interferences and therefore flagged as bad quality data.

The Probability distribution functions of the differences ΔSSS= SSS_{SMOS} -$SSS_{in\ situ}$ between SMOS L2 SSS and co-localized *in situ* SSS data are shown in Figure 1.c for ascending, descending and when merging both passes data over the global ocean. Considering the 95% percentile of the ΔSSS data, these distributions are found to be close to normal distributions (see dashed fits in Fig. 1c), with first and second order moments provided in Table I. Over the second half of 2010, 95% of the SMOS Level 2 products thus exhibit a global mean error of 0.52 with a standard deviation of 1.3 . In the tropical ocean, the mean error decreases to about 0.3 with a standard deviation of 1.

SMOS Level 2 SSS measured in ascending and descending passes are found in general too salty by 0.8 and 0.1 , respectively. This is not true when considering only the tropical oceans, for which the mean Satellite SSS are here too fresh by about 0.2 in descending passes.

The standard deviation of the error is however found to be systematically lower for ascending orbits (1.1 globally and 0.8 in the tropics) than for the descending ones (1.4 globally and 1.1 in the tropics).

As illustrated in Figure 1.d, which shows the average and standard error deviation as function of ±0.25 pss bins of *in situ* SSS values, SMOS data are in average significantly too salty in fresh waters below 33 . These observed global biases for fresh waters are mostly associated with measurements conducted in the North Pacific ocean, in the Labrador sea, as well as by those performed in the bay of Bengal.

B. *Spatio-temporal drifts in the retrieved SSS*

While the previous statistics give a first indication of the overall quality of the Level 2 products, they are based on a 6 months period over which significant temporal or spatial drifts may have occurred for several reasons (badly accounted for seasonal cycle in the forward model brightness temperature contributions, instrumental drifts, varying solar radiation impacts etc..) that may bias the overall statistics. To investigate this issue, the daily error statistics (mean and standard deviation) of the Level 2 products were evaluated using the ~300 match-ups/day and we applied to the results a 10-day running mean window filter to smooth them out. The latter are shown in Figure 2 and reveal several aspects of the data. First, the error standard deviation is seen to be approximately stable along the period. However, this is not the case for the 10-days averaged mean errors that are seen to significantly fluctuate from July to end December. The latter mean global biases are in general smaller for descending

passes than for ascending passes. The 10-days averaged global biases for both data set exhibit a fluctuation amplitude with time reaching a maximum value on the order of 1.2 over the period. These large temporal fluctuations in the mean errors are dominantly induced by a change in the Level 1-Level 2 processors versions occurring in July and at the beginning of August. The cross over in the mean errors between ascending and descending passes is indeed observed at the beginning of August. This is attributed to a change in the Level 1 processor that followed after a deep sky calibration update, and which was implemented in the L1 processor. The temporal fluctuations of the mean error after that date, period for which the L1 and L2 processor configurations were kept unchanged, nevertheless exhibit an amplitude standard deviation of 0.3 and 0.5 for ascending and descending passes, respectively. The amplitude of the temporal fluctuations of the running mean ΔSSS is found maximum during the period July to mid-October. More details about these drifts are obtained by analyzing the temporal evolution of the meridional averages of the ΔSSS. The latter were estimated over 1°-wide latitude bands with a 10-days running mean windows. As illustrated by the Hovmöller diagrams given in Figure 3, the temporal drifts affecting the retrieved SSS in ascending passes are almost independent of latitude, except for the southern latitude bands were a varying positive bias is detected. As will be shown later, the latter is associated with the impact on the SMOS measurements of the sea ice extent seasonal changes. However, the descending passes case shown in Figure 3a reveals a clear latitudinally dependent variation of ΔSSS with time for these orbits. A strong North-South variation in the retrieved SSS error is found starting mid-October until the end of the year. In December, this very strong bias reach a maximum amplitude of about 4-5 from South to North, varying from about -2 s for the latitude bands centered around 40°N up to +2 around 50°S. The sign change in this latitudinal bias occurs at a latitude that is seen to evolve from about 10° S at the beginning of October to about 30°S at the end of December. The spatio-temporal drifts in SMOS L2 SSS error found in the Hovmöller diagrams show that the previously derived overall SMOS L2 error statistics at global scale, may hide very significant local biases in the retrieval and shall therefore be taken with care.

C. SMOS retrieved SSS error major Geophysical Dependencies

The sea surface roughness impact on the L-band emissivity is known to be a potential major source of forward modeling errors for the spaceborne remote sensing of sea surface salinity. The sensitivity of emissivity to salinity is expected to decrease significantly in cold waters. To identify the potential impact of these two major geophysical error sources on the ΔSSS values, the latter were bin-averaged as function of the Level 2 processor ECMWF surface wind speed products (bin width of 1 m/s) and temperatures (bin width of 2°C). The results illustrated in Figure 4 reveal a systematic overestimation of the SMOS retrieved SSS at wind speed higher than ~13-14 m/s, with an increased bias magnitude as

the wind speed increases. As well, significant differences between SMOS and in situ observations are detected for wind speed lower than about 3 m/s, with ΔSSS values changing by about 2 from calm sea to conditions with 2-3 m/s wind speeds. In the dominant wind conditions from 4 to 12 m/s, no clear dependence of the SMOS L2 SSS biases with surface wind speed are however evidenced for both passes.

Although the data dispersion is quite large, a continuous degradation of the SSS retrieval quality is observed as the sea surface temperature diminishes. This is particularly clear below 6-7°C in ascending passes, which is a known threshold SST range below which sea ice may be present. Interestingly, there is no apparent degradation at low SST in descending passes. Most of these spurious data are likely associated with errors in the SMOS brightness temperature that occur at the transition between Antarctica and the open ocean. Nevertheless, considering a linear fit of the ΔSSS statistics as function of SST for both passes, SMOS L2 SSS mean error is found to increase with decreasing SST at a rate of about 0.05 pss/°C. Another major geophysical source of error in the SMOS Level 2 SSS product was identified as the modeling of the galactic signal reflection. We show in Figure 5 a first visual evidence of this problem. Based upon the modeling studies for SMOS mission [8], the impact is expected to be largest for descending passes in September because for these passes, the reflections of the instrument viewing directions over the field of view tend to lie along the galactic equator, where L-band galactic emission is maximum. In Figure 5a, we show an image of the SMOS Level 2 SSS retrievals for the descending passes of the 25th of September. Note the blue (too fresh) along-track strips in the retrieved Level 2 SSS that can be attributed to an underestimation of the modeled galactic signal reflection on the sea surface (see Figure 5b). Indeed, the higher the brightness temperature residual after correction, the fresher the retrieved SSS. These modeling errors might affect the quality of the retrieved SSS in descending passes from mid-August to mid-October, period over which the reflected galactic equator crossed the FOV.

D. SMOS Level 3 SSS quality

In order to better determine the overall Level 2 SSS quality, to further evaluate permanent non-identified errors at Level 2 and *in fine*, to estimate if the products meet the mission requirements, spatio-temporal averaging of the Level 2 products is necessary. The latter products were therefore aggregated over different spatial resolutions varying from 0.25° to 1°, and over 1 month (so-called Level 3 products). These Level 3 products were obtained using a simple averaging method. While more sophisticated methods can be used, this simple aggregation strategy is sufficient to illustrate the major and systematic problems found in the data.

In Figure 6, the evolution of the Level 3 products derived at a nominal spatial resolution of 0.25° for each month of the second half of 2010 is shown as function of pass-type (ascending and descending). Three major problems can be

visually detected in these Level 3 SMOS products.

First, SMOS SSS data are permanently flagged as bad and removed in several large world ocean area due to the presence of man-made radio frequency interferences. A major contaminated zone is the Northern ocean latitudes, particularly in ascending passes, for which a belt of spurious retrievals is systematically found, spanning North Pacific and Atlantic oceans, from the Bering sea to the North Sea. An analysis of the brightness temperature signals (not shown here) revealed that this permanent contamination is found to be induced by signal from a radar array located in North America, at the southern tip of Greenland and at several locations in England. Other strongly and often contaminated ocean areas are the Northern Indian Ocean, particularly the Arabian Sea and within a ~800 km wide belt along the Pacific coasts of Asia. While not clearly visible in the monthly averaged Level 3 products, many other ocean area are also affected by local but weaker or more intermittent RFI contaminations emanating from the coasts, particularly around the major coastal cities of the world.

A second major problem is the fact that SMOS SSS data are systematically biased (in general too salty) within a ~1500 km wide belt along the world coasts and sea ice edges, with a contamination intensity and spread strongly varying from ascending to descending passes. The signature of this so-called 'land-induced' contamination is seen to be very stable from month to month along the second half of the year. A more detailed analysis of this signal is given at the end of this section.

Finally, the previously identified L2 SSS spatio-temporal drifts are now clearly evidenced at Level 3. This is particularly true for the latitudinal biases found in descending orbits, with maximum magnitude reached at the end of the year and which translates into a significantly too fresh and too salty satellite SSS in the Northern and Southern oceans, respectively.

Despite these serious problems in the data, an error analysis of the SMOS Level 3 products has been conducted using the monthly data aggregated at 1° resolution. However, given the detected spatio-temporal drifts, the statistical error analysis is conducted separately for each month and each pass types. Results of the statistical analysis are provided in table II for the global ocean and table III for the tropical oceans. Considering all match-up data for a given selection (e.g. those for the month of august and ascending passes), it was found that the probability distribution of the ΔSSS for these Level 3 products is far from normality with significant skewness and kurtosis values, principally due to a high density of significant outliers. Considering the 90% percentile of the ΔSSS values, distributions become closer to Gaussian ones with first four moments provided in the tables. As illustrated 90% of SMOS Level 3 data over the global ocean exhibit a monthly error standard deviation on the order of 0.46 and 0.57, for ascending and descending passes, respectively. While the monthly error standard deviation is approximately stable in ascending passes, the higher value found in descending

passes is clearly attributed to the temporal and latitudinal drifts observed from October to December, which induce an increase of the monthly standard deviation error up to 1.1 at the end of the year. In the Tropical oceans, the SMOS Level 3 SSS standard deviation error is on the order of 0.38, except for the months of October and November in descending passe,s for which it reaches 0.5-0.6.

To investigate the averaged impact and extent of the land contamination on the Level 3 products, ΔSSS values where further binned as function of the distance to coast, estimated from an USGS land mask. The results shown in Figure 7 reveal that the median values of ΔSSS and its standard deviation generally increase as SMOS data are retrieved within approximately 1500 km from the coasts. The enhancement of the median ΔSSS as function of the distance to coast is more clearly seen in descending passes, with a continuous increase as the data get closer to the coast, reaching an amplitude of ~0.7 at about 150 km from the coasts. While the amplitude of the ΔSSS variation within 1500 km from coast is similar for ascending passes than for the descending ones, no continuous trend is observed as the data get closer to the coast. Note that the increase of the error standard deviation within the 1500 km coast-following belt may be associated with a strong decrease in the number of in situ observation, as one get closer to the coast.

A more precise view of the spatial extent and impact of the land contamination is obtained by plotting the spatial distribution of the 6 month period-averaged ΔSSS per 1° boxes. As seen in Figure 6, the land contamination extent and intensity seems apparently very stable as function of time. To minimize the potential impact of the temporal drifts on the average ΔSSS along the coasts, spatial distributions of the Level 3 ΔSSS were therefore adjusted so that the global distribution for each month and each pass type exhibit a zero mean value. This adjustment was performed using the monthly global mean errors provided in table II. The residuals were then averaged over the six months and are shown in Figure 8. This plot reveals that the land-contamination is locally worse than could be deduced from the globally averaged results shown in Figure 7. After removing the monthly mean errors, the residual ΔSSS amplitude along the world coast is generally larger than ±1. Moreover sign changes in the ΔSSS within the 'coastal-belt' can be observed with varying signatures in ascending and descending passes as function of the coasts considered. Too salty SMOS retrievals (by more than 1) are found along most of the world coasts (e.g., West coasts of America, Europe and Africa; North coasts of Australia, South-America and Indonesia in ascending passes; coasts of South Africa, America and South Australia in descending passes). Nevertheless, some area along the world coasts also indicate too fresh retrieved salinities, particularly in ascending passes such as area along the South Australian coasts, along most east coasts of America and Africa as well as in the proximity of Asia eastern Pacific coasts.

Prior to launch, several studies [e.g., 18] estimated that a contamination of the reconstructed brightness temperatures at the ocean/land transition could seriously affect the quality of SSS retrieval only within a coastal band of ~100-150 km (2-3 pixels) width. The observed 'land contamination' effect seen in SMOS data is actually much more important than previously anticipated. During the last six months, ESA team members and scientists looked for the potential source of this problem and it was recently found that a very likely source was a bug in the Level 1 processor evaluation of the DC component of the visibilities. As will be illustrated in part II, a much reduced contamination is found using a corrected version of the Level 1 processor.

IV. SUMMARY AND DISCUSSION

In the first part of this paper, the results of an analysis of the quality of the first operational SMOS Sea Surface Salinity (SSS) products have been presented. To assess this quality, *in situ* SSS data were collected in the upper 10 m of the global ocean over the second half of the year 2010. These *in situ* data originate from several sources such as the ARGO floats array, CTD sensors, Mooring array in the Tropics and Thermosalinograph instruments on board ships of opportunity. The ensemble data set was qualified and provide a very dense distribution of measurements, that were further co-located with SMOS Level 2 swath SSS data for the purpose of validation.

Over the second half of 2010, 95% of the SMOS Level 2 products are found to exhibit a global mean error $\Delta SSS=SSS_{SMOS}-SSS_{in\ situ}$ of 0.52 with a standard deviation of 1.3 . In the tropical oceans, the mean error decreases to about 0.3 with a standard deviation of 1 . The error standard deviation is found to be systematically less for ascending orbits (1.1 globally and 0.8 in the tropics) than for the descending ones (1.4 globally and 1.1 in the tropics) . Classifying the errors as function of SSS values themselves, a systematic too salty satellite SSS for the fresh oceanic waters below 33 was found, which is dominantly attributed to errors located in the fresh North Pacific and Atlantic, as well as in the Bay of Bengal areas.

The evolution of the 10-days averaged ΔSSS 95% percentil statistics (global mean and standard deviation) of the Level 2 products was studied from the match up database and reveal several aspects of the data. First, the standard error deviation is seen to be approximately stable along the period. However, this is not the case for the 10-days averaged mean errors that are seen to significantly fluctuate from July to end December. The latter mean global biases are in general smaller for descending passes than for ascending passes and exhibit a fluctuation with time reaching a maximum amplitude on the order of 1.5 over the period. These large temporal fluctuations in the mean errors are dominantly attributed to changes in the

Level 1-Level 2 processors versions occurring in July and at the beginning of August. Nevertheless, after this last processor updates, the retrieved salinities mean errors are still fluctuating with time with an amplitude standard deviation on the order of 0.3-0.5 .

More details about these drifts were obtained by analyzing the temporal evolution of the meridional averages of the ΔSSS. The latter were estimated over 1°-wide latitude bands with a 10-days running mean windows. As found, the temporal drifts affecting the retrieved SSS in ascending passes are almost independent of latitude, except for the southern latitude bands due to the sea ice extent seasonal changes. However, a strong 4-5 North-South variation in the retrieved SSS error is found for descending passes starting mid-October until the end of the year, varying from about -2 for the latitude bands centered around 40°N up to +2 around 50°S.

Major geophysical dependencies of the ΔSSS were then analyzed considering only SMOS data generated with roughness model 2, developed by the first two authors of this manuscript [11]. The observed dependencies reveal (i) that for the dominant wind conditions, the SMOS Level 2 errors are weakly dependent on sea surface wind speed. Significant biases are however detected in the low (below 3 m/s) and high (over 14 m/s) wind speed regimes. As expected from the kown evolution of the L-band emissivity sensitivity to SSS with SST, a continuous degradation of the SMOS SSS retrieval quality is observed as the sea surface temperature diminishes. SMOS L2 SSS mean error is thus found to increase with decreasing SST at a rate of about 0.05 pss/°C. This is particularly clear below 6-7°C, a known threshold SST range below which sea ice may be present. However, the errors in these relatively cold seas are seen to vary significantly from ascending to descending passes, which indicates that the low L-band sensitivity of surface emissivity to SSS in cold seas is not the first factor responsible for the errors, and that other effects might be the sources for these errors ('land-contamination' at the Antarctica/open ocean transitions, sea ice contamination, high winds model biases, lack of data due to increased rfi contaminations in northern latitudes..). Another major geophysical source of error in the SMOS Level 2 SSS product was identified as the modeling of the galactic signal reflection. As shown, too fresh salinity are retrieved when the strong galactic equator sources reflect in the Field of view, indicating an underestimation of that modeled contribution. These modeling errors affect the retrieved SSS in descending passes from mid-August to mid-October, period over which the reflected galactic equator crosses SMOS FOV.

In order to better determine the overall Level 2 SSS quality, to evaluate permanent flaws non-identified at Level 2 and to estimate if the products meet the mission requirements, spatio-temporal averaging of the Level 2 products was conducted considering one month duration over spatial boxes of 1°x1°. A simple averaging method was used for aggregation of the L2 products.

Three major problems were detected in these simply derived Level 3 SMOS products. First, occurrence of radio frequency interferences at L-band is found to be a major issue over the oceans. The latter contaminations permanently disable SSS retrievals in many ocean areas, particularly in the Northern latitudes in ascending passes, in the Arabian sea and along the Pacific coasts of Asia. A second major problem is the fact that SMOS SSS data are systematically biased (in general too salty) within a ~1500 km wide belt along the world coasts and sea ice edges. The intensity of that contamination and its spread are strongly varying from ascending to descending passes, and increases in magnitude as the pixels considered lie closer to the coasts. The signature of this so-called 'land-induced' contamination is seen to be very stable from month to month along the second half of the year.

Third, the previously identified L2 SSS spatio-temporal drifts are clearly evidenced at Level 3. More critical are the latitudinal biases found in descending orbits, with maximum magnitude reached at the end of the year and which translates into a significantly too fresh and too salty satellite SSS in the Northern and Southern oceans, respectively. The existence of such latitudinal bias in descending passes, varying as function of time, is critical for Level 3 product generation. Indeed, they currently limit our ability to exploit the combination of ascending and descending passes measurements, in view of maximizing the SSS error reduction at Level 3.

In this context, 90% of SMOS SSS data aggregated over 1°x1° boxes for 1 month duration (so-called Level 3 products) nevertheless exhibit an error standard deviations on the order of 0.46 and 0.57 , for ascending and descending passes, respectively. While the monthly error standard deviation is approximately stable from month to month in ascending passes, the higher value found in descending passes is clearly attributed to the temporal and latitudinal drifts observed from October to December. In the Tropical oceans, the SMOS Level 3 SSS standard deviation error is on the order of 0.38 , except during the period from October to November for the drifting descending passes, for which it reaches 0.5-0.6 .

It is important to recall here that the SMOS polarimetric interferometric radiometry technique is used for the first time in the context of earth observation from space. Retrieving sea surface salinity from interferometric radiometer measurements of upwelling L-band radiation is a very challenging objective and the validation exercise conducted here reveals that a significant effort is still required to improve the quality of the first SSS retrieval attempts from SMOS data, in order to reach the mission requirements. While the overall error statistics is promising, issues of major concerns are 'land-contamination', spatio-temporal drifts; forward modeling errors and radio-frequency interferences impacts. The fact that the instrument components and the reconstructed brightness temperature may exhibit some temporal drifts to within ±0.5 was anticipated before launch and could be adjusted by vicarious calibration, as was done previously for other passive satellite

measurements. Nevertheless, occurrences of time varying latitudinal variations in the retrieved SSS, such as the ones observed in descending passes at the end of the year are critical in view of reducing the satellite SSS error at Level 3. Identification of the sources for the latter spurious signals and associated corrections are clearly needed.

The observed 'land contamination' effect seen in the first set of SMOS operational SSS data is a very critical issue for science applications as most of the important oceanic variability in SSS is found within 1000 km from the coasts (largest river run off, west and east boundary currents, ..). However, this is now known to be associated with a bug in the used version of the Level 1 processor. Accordingly, the land contamination will be strongly minimized in the future reprocessed SSS data based on a corrected version of the Level 1 processor.

Given the complexity of the instrument and the numerous problems found in the data, it is clear that satellite retrieved SSS comparisons with *in situ* data alone, while necessary to first assess the quality of the satellite retrievals is not a sufficient exercise to understand and characterize all the major sources for the problems detected and to propose algorithm improvements. In this Part I, we aimed at providing the reader with an overview of the current quality of the currently produced SMOS Level 2 SSS data and to point out some major flaws in the data.

A deeper analysis of the sources for the observed land-contamination, drifts and modeling errors is thus needed in term of brightness temperature signal dependencies. An attempt in this sense is proposed in Part II of the present work.

REFERENCES

[1] J. Font, A. Camps, A. Borges, M. Martín-Neira, J. Boutin, N. Reul, Y. H. Kerr, A. Hahne, and S. Mecklenburg (2010), SMOS: The

Challenging Sea Surface Salinity Measurement from Space, *Proceedings of the IEEE* , vol 98, 5,649-665.

[2] S. H. Yueh, West, R., Wislon W.J., Li, F.K., Njoku, E.G. and Rahmatsamii,Y., (2001), Error sources and feasibility for microwave remote sensing of ocean surface salinity. *IEEE Transactions on Geoscience and Remote Sensing,* 39, pp. 1049-1060.

[3] E. P. Dinnat, J. Boutin, G. Caudal, and J. Etcheto, "Issues concerning the sea emissivity modeling at L band for retrieving surface salinity," Radio Sci., vol. 38, no. 4, 8060, 2003, DOI:10.1029/2002RS002637.

[4] J. Boutin, P. Waldteufel, N. Martin, G. Caudal, and E. Dinnat, Surface salinity retrieved from SMOS measurements over global ocean: imprecisions due to surface roughness and temperature uncertainties, Journal of Atmospheric and Oceanic Technology, 21, 1432-1447, 2004.

[5] A. Camps, Vall-llossera, M., Villarino, R., Reul, N., Chapron, B., Corbella, I., Duffo, N., Torres, F., Miranda, J.J., Sabia, R., Monerris, A., and R. Rodriguez, R (2005), The emissivity of foam-covered water surface at L-band: Theoretical modeling and experimental results from the FROG 2003 field experiment, *IEEE Trans. Geosci. Remote Sens.*, 43, 925–937.

[6] N. Reul, J. Tenerelli, N. Floury and B. Chapron, "Earth Viewing L-Band Radiometer sensing of Sea Surface Scattered Celestial Sky Radiation. Part II: Application to SMOS", IEEE Transactions on Geoscience and Remote Sensing, vol 46, 3, doi:10.1109/TGRS.2007.914804, 2008.

[7] J. E. Tenerelli, N. Reul, A. A. Mouche, and B. Chapron, "Earth-viewing L-band radiometer sensing of sea surface scattered celestial sky radiation—Part I: General characteristics," IEEE Trans. Geosci. Remote Sens., vol. 46, no. 3, pp. 659–674, Mar. 2008.

[8] N. Reul, J. Tenerelli, B. Chapron and P. Waldteufel, "Modelling Sun glitter at L-band for the Sea Surface Salinity remote sensing with SMOS", *IEEE Transactions on Geoscience and Remote Sensing*, vol 45, No 7, pp 2073-2087, 2007.

[9] C.S. Ruf, Swift, C.T., Tanner, A.B. and Le Vine D.M., (1988), Interferometric synthetic aperture microwave radiometry for the remote sensing of the Earth. IEEE Transactions on Geoscience and Remote Sensing, 26, pp. 597-611.

[10] S. Mecklenburg S., N. Wright, C. Bouzinac and S. Delwart (2009), Getting down to business - SMOS operations and products, *ESA Bulletin*, 137, 25-30.

[11] S. Zine, J. Boutin, J. Font, N. Reul, P. Waldteufel, C. Gabarró, J. Tenerelli, F. Petitcolin, J. L. Vergely, M. Talone, and S. Delwart, "Overview of the SMOS sea surface salinity prototype processor," IEEE T. Geosci. Remote, vol. 46, pp. 621-645, 2008.

[12] T. P. Boyer, Antonov, J.I. , Garcia, H.E., Johnson, D.R., Locarnini, R.A., Mishonov, A.V., Pitcher, M.T., Baranova, O.K. and Smolyar, I.V., (2006), *World Ocean Database 2005*. U.S. Government Printing Office, Washington, D.C., DVD.

[13] J. Font et al., SMOS first data analysis for sea surface salinity determination, submitted to *Int. Journal Rem. Sens.*, 2011.

[14] J. E. Tenerelli, N. Reul, and B. Chapron, Analysis of SMOS Brightness Temperatures Obtained from March through May 2010, Proceedings of the ESA Living Planet Symposium, June 28 – July 2, Bergen, Norway. ESA Special Publication SP-686(2010).

[15] J. Boutin, N. Martin, X. Yin, N. Reul, P. Spurgeon, First assessment of SMOS measurements over open ocean: part II Sea Surface Salinity, submitted to *IEEE T. Geosci. Remote Sens.*, 2011.

[16] F. Gaillard, E. Autret, V.Thierry, P. Galaup, C. Coatanoan, and T. Loubrieu , 2009. Quality control of large Argo data sets. *Journal of Atmostpheric and Oceanic Technology*, 26(2), 337–351.

[17] E. Brion, F. Gaillard, L. Petit de la Villéon, T. Delcroix, G. Alory, G. Reverdin, 2010. GLOSCAL: In-Situ datasets and gridded fields

for calibration and validation of SMOS. Poster and paper in symposium proceedings, ESA-Living Planet Symposium, Bergen, 28 june to 2 july 2010.

[18] S. Zine, J. Boutin, P. Waldteufel, J. L. Vergely, and P. Lazure: "Issues about retrieving sea surface salinity in coastal areas from SMOS data". IEEE Transactions on Geoscience and Remote Sensing, 45, 10.1109/TGRS.2007.894934, 2007.

Nicolas Reul received the B.S. degree in marine science engineering from Toulon University, La Garde, France, in 1993, and the Ph.D. degree in physics (fluid mechanics) from the University of Aix-Marseille II, Marseille, France, in 1998. From 1999 to 2001, he worked as a Postdoctoral Researcher with the Applied Marine Physics Department, Rosenstiel School of Marine and Atmospheric Science, University of Miami, Coral Gables, FL. Since 2001, he has been a Research Scientist with the Spatial Oceanography Group, Institut Français de Recherche pour l'Exploitation de la Mer, Plouzané, France, where he is responsible for the activities concerning the SMOS satellite mission and the associated research on sea surface salinity remote sensing from Space. The focus of his research program is to improve the understanding of the physical processes at air–sea interface and passive/active remote sensing of the ocean surface. He has experience in applied mathematics, physical oceanography, electromagnetic wave theory, and its application to ocean remote sensing.
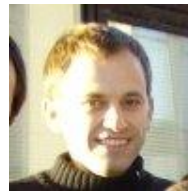
Joseph Tenerelli received a B.S. in Atmospheric Sciences from the University of Washington in 1994. From 1999 to 2005 he was a Research Associate at the Rosenstiel School of Marine and Atmospheric Science, University of Miami, where he worked as part of a team to develop a coupled atmosphere-ocean-surface wave model with vortex-following mesh refinement suitable for simulating hurricanes. In April 2005 he joined IFREMER (Brest, France) as a research engineer working as part of a team developing an algorithm to retrieve sea surface salinity from L-band radiometric measurements (the European Space Agency's SMOS project). Since 2008 he has continued his work on the SMOS mission as a research engineer within the Radar Division of Collecte Localisation Satellites.

Jacqueline Boutin received the Ph.D. degree in physical methods in remote sensing from the University Paris VII, Paris, France, in 1990. She is currently a Research Scientist at the Centre National de la Recherche Scientifique (CNRS) in the Laboratoire d'Océanographie et du Climat— Expérimentation et Approches Numériques (LOCEAN), Paris. She has widely studied the validity of remotely sensed wind speeds and the ocean/atmosphere exchange of CO_2 at large scale using both satellite (wind speeds, sea surface temperature, and ocean color) and in situ data (in particular, carbon-interface ocean–atmosphere autonomous drifters, CARIOCA). Since 1999, she has been involved in the preparation of the SMOS mission. She participated in the development of an L-band sea surface emissivity model and in several airborne campaigns (WISE and Eurostarrs). She is a member of the European Space Agency Expert Support Laboratories that define and validate the processing of SMOS Level 2 measurements for the retrieval of sea surface salinity.

Bertrand Chapron received the Ph.D. degree in Physics (Fluid Mechanics), IRPHE, University Aix-Marseille II (1988) and the B. Eng, Institut National Polytechnique Grenoble(1984) He spent 3 years as a post-doctoral research associate at the NASA/GSFC/Wallops Flight Facility, USA. He has experience in applied mathematics, physical oceanography, electromagnetic wave theory and its application to ocean remote sensing.Bertrand Chapron, research scientist, is presently head of the Spatial Oceanography group at IFREMER, Institut Francais de Recherche et d'Exploitation de la MER, responsible of the CERSAT, Centre ERS Archivage et Traitement. CoI or Pi in several ESA (ENVISAT, Global Navigation Satellite System), NASA and CNES CNES (TOPEX/POSEIDON, JASON) projects. Co-responsible (with H. Johnsen, NORUT) of the ENVISAT ASAR-Wave Mode algorithms and scientific preparation for the ENVISAT wind and wave products.

science team and contributed to the development of the Argo project in France. She now works with the 'Service d'observation ARGO' at Laboratoire de Physique des Océans (Brest) where she developps tools for data synthesis and carries research projects. She participated to numerous national scientific committes. Her research interest include the monitoring of the global ocean to study interannual to decadal variability of the heat and fresh water content and the analysis of the circulation of intermediate waters in the North-Atlantic.

Frédéric PAUL holds an engineering diploma in Computer Science ('04) from the Ecole Nationale d'Ingénieurs de Brest, France. He works since '06 in the Center for Satellite Exploitation and Research (Ifremer, Brest) as software architect, where he is responsible for the design, development and integration of multi-mission tools to manage satellite data for operational oceanography and research projects. He focuses on new technologies based on big data concepts and cloud computing to build scalable processing infrastructures at petascale.

Emilie Brion have worked as a research assistant with the 'Service d'observation ARGO' at IFREMER Laboratoire de Physique des Océans (Brest) where she developped tools for in situ data validation and synthesis She now works at the private company Atlantide in Brest.

Olivier ARCHER is an expert in Computer Science and works since in the Center for Satellite Exploitation and Research (Ifremer, Brest) as software architect, where he is responsible for the design, development and integration of multi-mission tools to manage satellite data for operational oceanography and research projects. He focuses on new technologies based on big data concepts and cloud computing to build scalable processing infrastructures at petascale.

Fabienne Gaillard received the Ph.D. degree in physical oceanography from the Universiy of Bretagne occidentale, Brest, in 1983. She was a Postdoctoral Research Associate at MIT from december 1983 to August 1985. In January 1986, she joined the Departement Etudes Oceaniques at Ifremer, Brest, where she developed inverse modelling with application to underwater acoustict omography. She was contributing or principal investigator for several European projects (Thetis 1, Thetis 2, Canigo, Octopus). In 1999 she joined the Coriolis

TABLE I

SMOS LEVEL 2 ΔSSS 95% percentile error Statistics (pss) for the GLOBAL OCEAN AND TROPICAL OCEANS
(|lat|≤27.5°)

Statistics	Pass	Global	TROPICS
Mean	Asc	0.81	0.64
	Desc	0.1	-0.19
	Both	0.52	0.27
Standard Deviation	Asc	1.1	0.83
	Desc	1.4	1.1
	Both	1.32	1

[1]

TABLE II

SMOS LEVEL 3 1°x1° monthly average ΔSSS 90% percentile error Statistics (pss) for the GLOBAL OCEAN

Statistics	Pass	July	Aug	Sep	Oct	Nov	DEC
Mean	Asc	0.3	0.5	1.1	1.03	0.9	-0.71
	Desc	0.91	0.01	-0.32	-0.13	-0.38	-0.25
Standard Deviation	Asc	0.5	0.48	0.51	0.43	0.45	0.39
	Desc	0.5	0.54	0.44	0.61	0.91	1.1
Skewness	Asc	0.28	0.1	-0.06	0.07	0.01	-0.25
	Desc	-0.12	0.11	0.25	0.49	0.22	-0.025
Kurtosis	Asc	3.32	3.3	3.6	3	2.88	2.82
	Desc	2.76	2.47	2.7	2.7	2.2	1.8

TABLE III

SMOS LEVEL 3 1°x1° monthly average ΔSSS 90% percentile error Statistics (pss) for the TROPICAL OCEANS (|LAT|<27.5°)

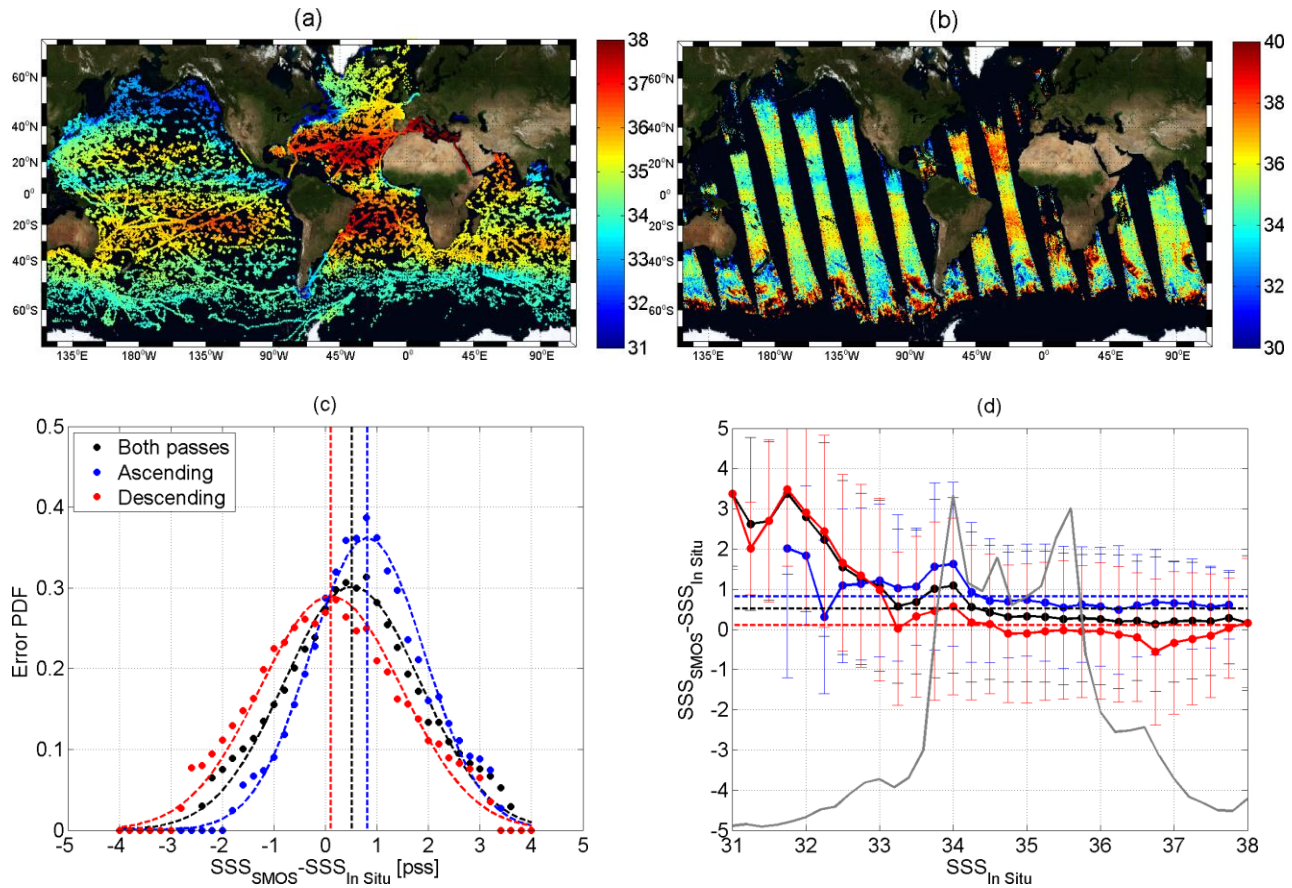| Statistics	Pass	July	Aug	Sep	Oct	Nov	DEC
Mean	Asc	0.2	0.48	1	0.85	0.67	0.59
	Desc	1.04	0.07	-0.42	-0.44	-0.88	-0.96
Standard Deviation	Asc	0.35	0.41	0.39	0.32	0.38	0.37
	Desc	0.39	0.4	0.37	0.38	0.5	0.6
Skewness	Asc	-0.06	0.02	-0.15	-0.06	-0.34	-0.09
	Desc	-0.12	0.11	0.25	0.49	0.22	-0.025
Kurtosis	Asc	3.9	3.5	3.8	3.2	3.5	3
	Desc	2.76	2.47	2.7	2.7	2.2	1.8

[2]
[3]
[4]
[5]
[6]
[7]
[8]

Figure 1:. (a) Spatial distribution of the ensemble of *in situ* qualified SSS data collected between July and December 2010 and used for SMOS Level 2 and 3 products quality assessment, (b) Example of one day of SMOS Level 2 ascending swath SSS retrieval products (4 August 2010). (c) Probability distribution function of the global differences $\Delta SSS = SSS_{SMOS} - SSS_{in\ situ}$ between SMOS L2 SSS and *in Situ* SSS. The dashed curves are Gaussian fit through the observed distributions. The dashed vertical lines indicates the mean values. All Data (Black), Ascending passes (blue) and Descending passes (red) (d) Mean ΔSSS values ± 1 standard deviation per bins of ± 0.25 of *in situ* SSS. The legend is the same than in (c). The gray curve is the histogram of *in situ* SSS values, scaled to fit within the plot.

[9]
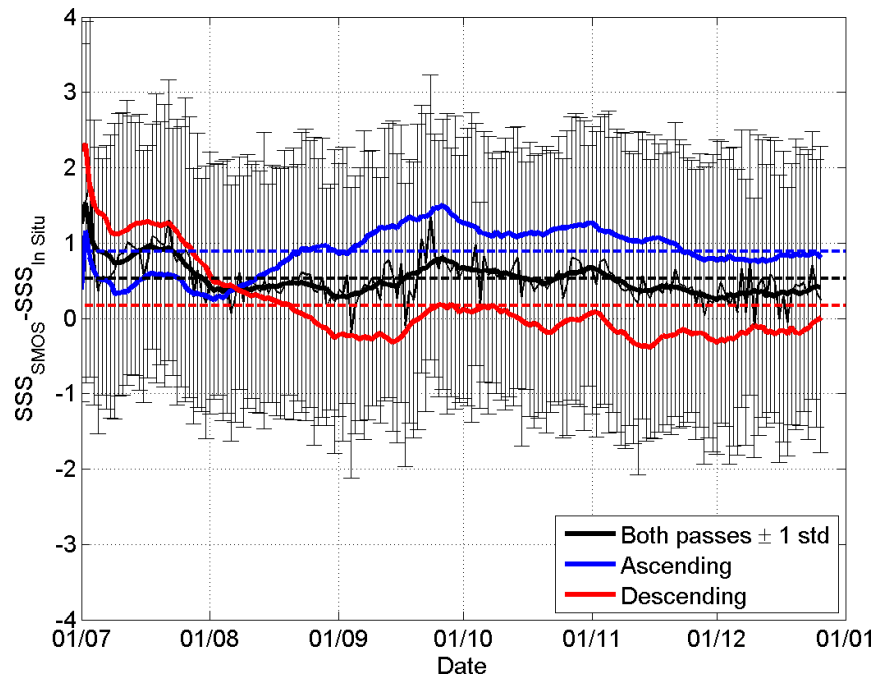
Figure 2: The black thin curve is showing the daily estimates of the globally averaged differences between SMOS Level 2 and in situ SSS over the period ranging from July to January 2010. The vertical bars are showing the ±1 standard deviation. The black thick curve is a 10-day running mean window of the daily and globally averaged difference. The blue and red curves are showing the 10-day running mean window of the daily and globally averaged difference for Ascending passes and Descending passes, respectively. The horizontal dashed blue and red lines are the annual averaged differences for ascending and descending passes, respectively.
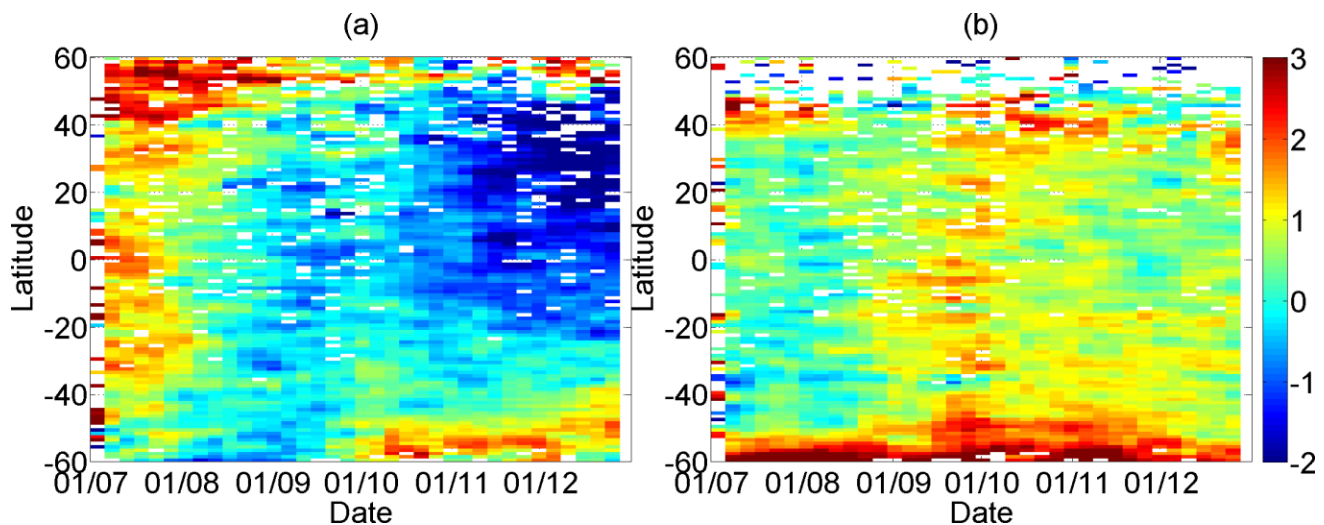
Figure 3: Temporal evolution from July 2010 to end December 2010 of the meridional average of ΔSSS. (a) Descending passes (b) Ascending passes. The color scale is in PSS.
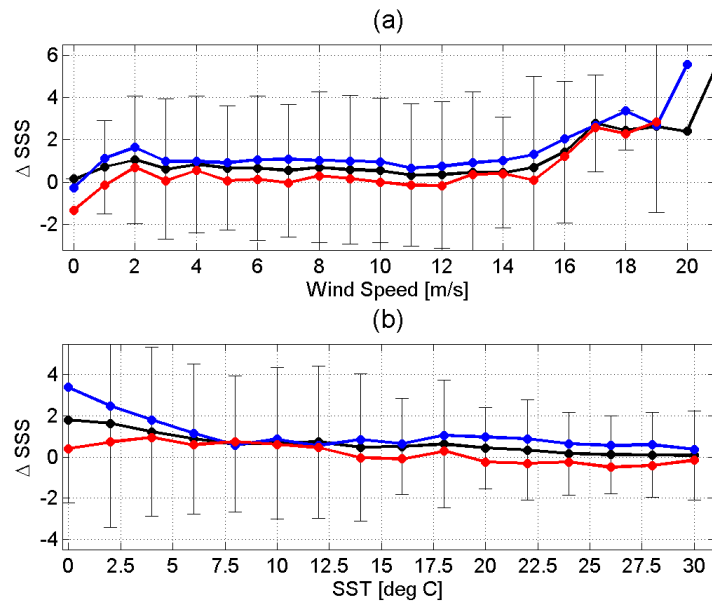
Figure 4: Binned-average values of ΔSSS= SSS$_{SMOS}$ -SSS$_{in\ situ}$ as function of ECWMF surface wind speeds per bins of 1 m/s (a) and as function of sea surface temperatures per bins of 2°C (b). All Data (Black), Ascending passes (blue) and Descending passes (red) . The vertical bars indicate ±1 standard deviation.
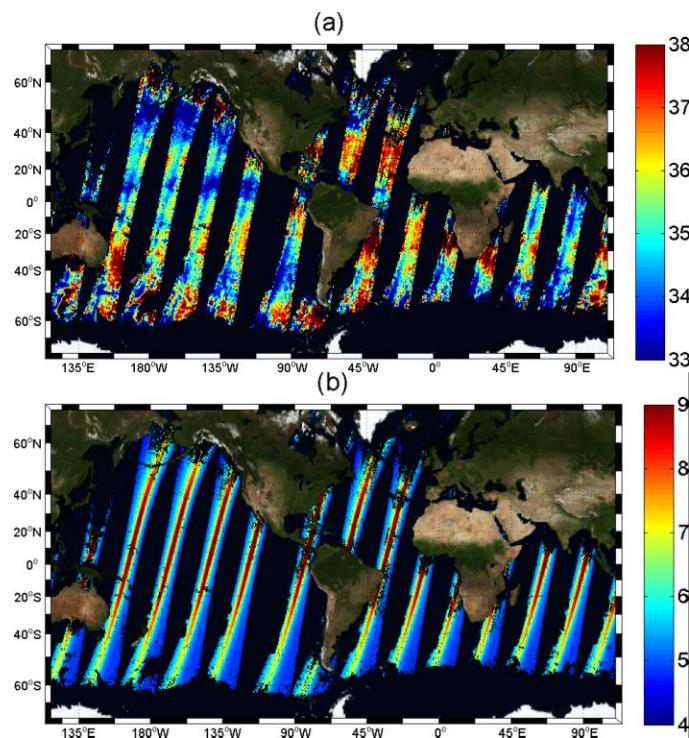

Figure 5: (a): Image of the SMOS Level 2 SSS retrievals for descending passes the 25th of september. Note the blue (too fresh) along-track strips due to bad correction of the galactic signal reflection on the sea surface. (b): Corresponding model predictions of the sea surface reflected galactic equator radiations for that period (Kelvins).

.
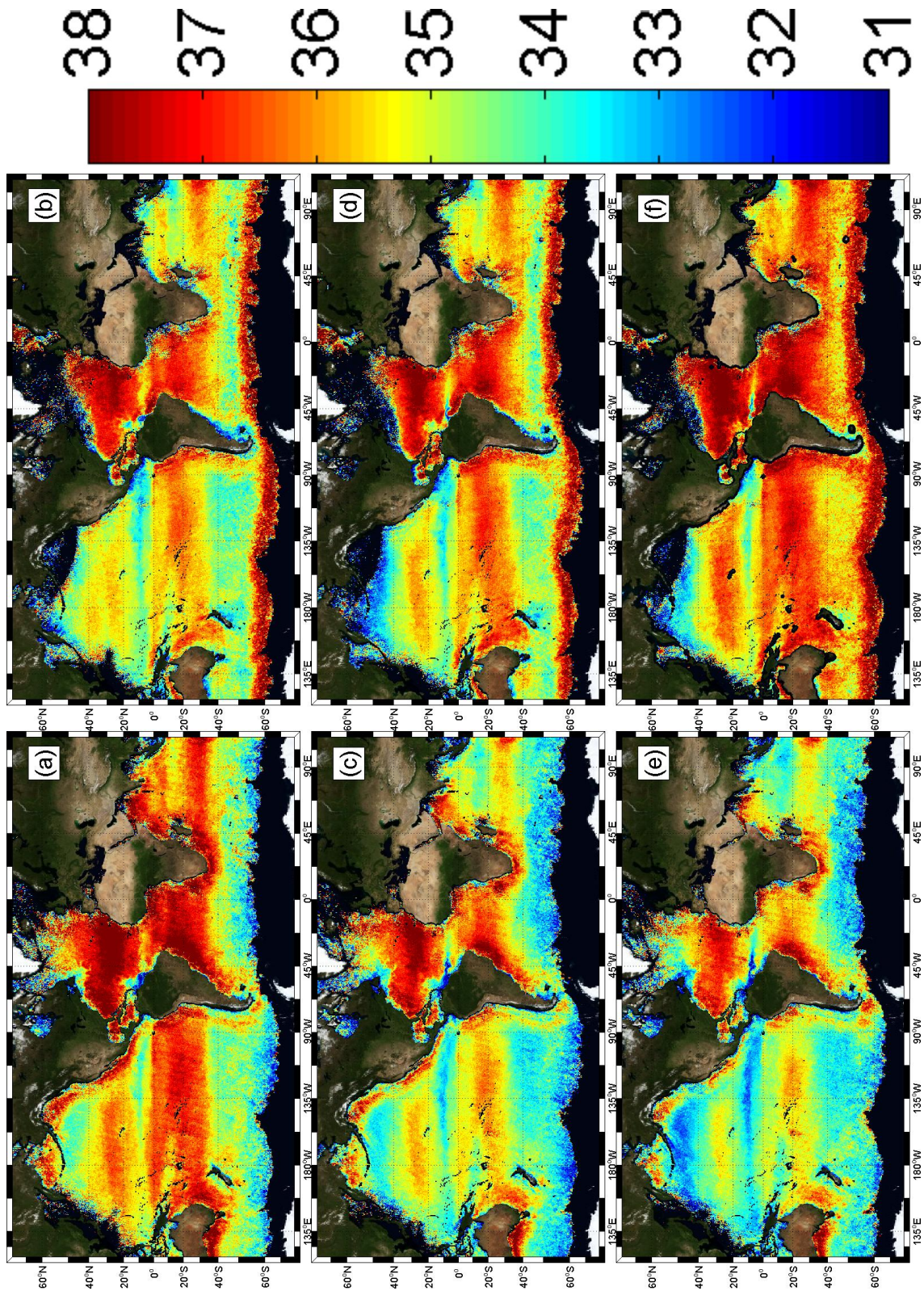
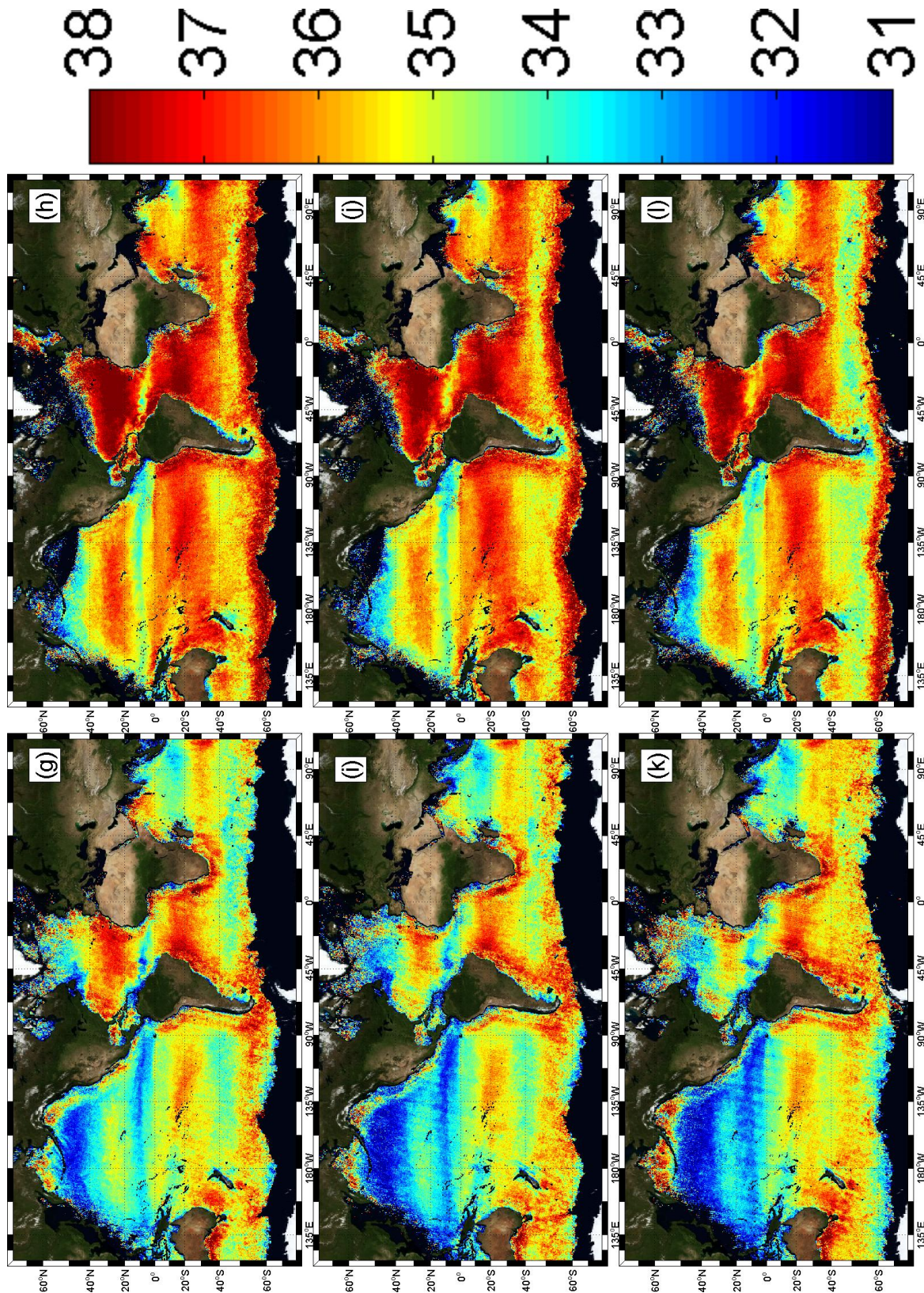**Figure 6**: see legend next page.

Figure 6 (continued) :Monthly average Sea Surface Salinity estimated from SMOS Level 2 SSS. (left) Descending passes (right) Ascending passes. (a-b) July; (c-d) August; (e-f) September; (g-h) October; (i-j) November and (k-l) December 2010. Spatial resolution is 0.25°x0.25°.
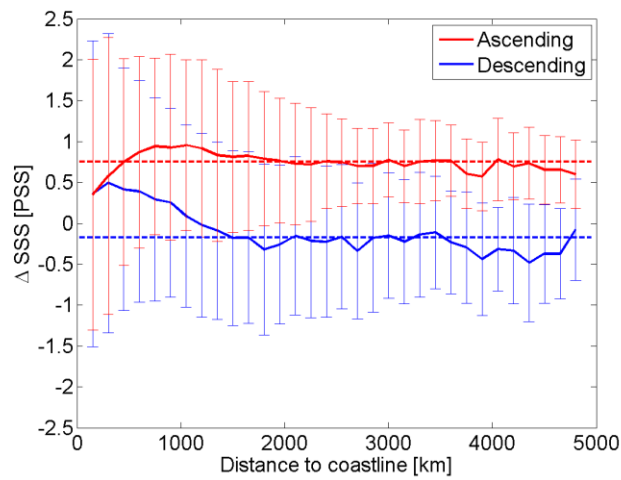
Figure 7. Median value of ΔSSS ±1 standard deviation as function of the distance to coastline for the period July to December.

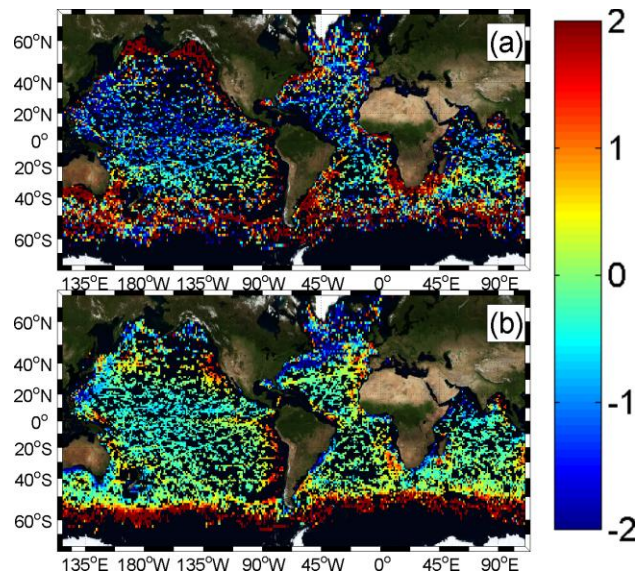**Figure 8**. Spatial distribution of the mean differences between SMOS Level 3 monthly-averaged SSS products at 1°x1° resolution and in situ data considering the period July to December 2010, after correcting SMOS data for the global mean temporal biases. (a) Descending passes (b) Ascending passes.